Thesis manuscript

Patellar tracking using a grid of skin-mounted markers evaluated by four-dimensional computed tomography

By Willem Zandee

4727851

Master Thesis Biomedical Engineering (BM51032)

Department of Biomechanical Engineering

Faculty of Mechanical, Maritime and Material Engineering

Delft University of Technology

To be defended on May 23rd, 2022

Thesis committee

Prof. dr. ir. J. Harlaar	TU Delft, supervisor
Dr. E.M. Macri	Erasmus MC, co-supervisor
Dr. M.G.H. Wesseling	TU Delft, co-supervisor
Dr. A. Seth	TU Delft, co-supervisor
Prof. dr. E.J.M. Veeger	Independent assessor

Uploaded to repository on 12-05-2022

Table of contents

Abstract

BACKGROUND: Research on the role of patellar biomechanics in patellofemoral (PF) joint pathologies requires accurate and reliable measurement of the patella relative to the femur (patellar tracking) but current methods have limitations. *In vivo* measurement of PF kinematics is done using medical imaging techniques but these are expensive, involve radiation exposure or only allow slow, supine motions. A widely used alternative is optical motion capture combined with musculoskeletal modeling. However, due to the large motion of the skin relative to the patella, the typical approach using anatomical calibrated skin-markers is unsuitable. As the shape of the patella is grossly visible underneath the skin, placement of a grid of skin-mounted markers on the skin covering the patella might offer an alternative for patellar tracking.

OBJECTIVE: The objective of this study was to develop a patellar tracking framework designed to measure *in vivo* PF translations using a grid of skin-mounted markers and to compare it to *in vivo* measures derived from dynamic CT images and musculoskeletal model estimates.

MATERIALS AND METHODS: Two participants performed a supine knee flexion-extension motion with a grid of 42 retroreflective markers placed on the right knee during four-dimensional computed tomography (4D-CT) measurement and optical motion capture. A patellar identification algorithm (PIA) was developed to estimate the PF translations in the medial – lateral (ML), superior- inferior (SI) and anterior – posterior (AP) directions. PF translations were determined by four different methods: CT bone geometry-based (CT_BONES), CT marker grid-based (CT_GRID), optical motion capture marker grid-based (OMC_GRID) and by musculoskeletal modeling (OMC_MODEL). To evaluate the feasibility of our method we first compared CT_BONES to CT_GRID. Next, results obtained by different measurement types (CT_GRID and OMC_GRID) and results obtained by two different marker-based methods (OMC_GRID and OMC_MODEL) were compared. To compare ranges of motions, patellar excursions relative to the femur were evaluated and compared for all knee angles (KA_ALL) and for knee angles > 20° (KA_ENGAGED).

RESULTS: Differences in patellar excursions given by CT_BONES and CT_GRID during KA_ENGAGED were less than 4 mm and RMSEs less than 3 mm. These differences were less than 5 mm between CT_GRID and OMC_GRID (RMSE: 5 mm) and less than 16 mm between OMC_GRID and OMC_MODEL (RMSE: 10 mm) for knee angles lower than 20°. Larger differences in patellar excursions and RMSEs were seen during KA_ALL.

CONCLUSION: PF translations could be measured using a marker grid with an accuracy within 3 mm for knee angles larger than 20° (i.e. during patellar engagement). However, our method performed worse for knee angles smaller than 20° flexion (an accuracy within 12 mm). The findings of this study provide valuable baseline knowledge for non-invasive, marker-based patellar tracking. Future studies should include larger sample sizes to allow for proper validation.

List of abbreviations

4D-CT	four-dimensional computed tomography
ACL	anterior cruciate ligament
ACS	anatomical coordinate system
AP	anterior – posterior
CT	computed tomography
CT_BONES	PF translations based on bone geometries provided by CT data
CT_GRID	PF translations based on marker grid trajectories provided by CT data
DOF	degree(s) of freedom
FE	finite element
ICP	iterative closest point
KA_ALL	all knee angles
KA_ENGAGED	knee angles in which the patella is engaged (all knee angles > 20°)
ML	medial - lateral
MRI	magnetic resonance imaging
MS	musculoskeletal
OMC	optical motion capture
OMC_GRID	PF translations based on marker grid trajectories provided by OMC
OMC_MODEL	PF translations based on musculoskeletal model simulation using OMC
PF	patellofemoral
PFOA	patellofemoral osteoarthritis
PFP	patellofemoral pain
PIA	patellar identification algorithm
RMSE	root mean squared error
SI	superior – inferior
STA	soft tissue artefacts

1. Introduction

1.1. Patellofemoral osteoarthritis

The lifetime risk of developing symptomatic knee osteoarthritis (OA) is 45% [1]. One out of two knee OA patients receive total knee replacement within their lifetime [2] and the resulting annual costs in the United States alone exceed 27 billion dollars [3]. The largest risk factors for disease development are aging and obesity, which is alarming since the general population is becoming older and more obese. Other risk factors include previous anterior cruciate ligament (ACL) injury [4], reconstructive surgery [5] and genetic susceptibility [6]. A diagnostic precursor for patellofemoral osteoarthritis (PFOA) is patellofemoral pain (PFP), which affects active, sedentary, young and old populations [7]. PFP and PFOA patients report a lower quality of life compared to healthy individuals as they experience problems executing daily activities. This highlights the importance of research on the development, progression and prevention of PF pathologies.

Altered PF joint mechanics are thought to contribute to the development of PFOA [8, 9, 10]. Therefore, current research focusses on the monitoring of *in vivo* changes in joint stress [11]. This has been done primarily using planar knee models [12] but two-dimensional models tend to neglect out-of-plane motion and do not capture the natural complexity of patellar movement in three dimensions [13]. Recent studies solved this by evaluating 3D knee mechanics by discrete element analysis [11], the finite element method [14] or musculoskeletal modeling [15, 16]. One important aspect all these approaches have in common is that PF joint kinematics – the relative motions of the patella and the femur - are used to calculate PF stress. This is because PF stress is determined by the articulating forces that the femur and patella exert on each other, and these are a result of PF kinematics. This shows the importance of valid and reliable measurement of the patella's location with respect to the femur, which is referred to as patellar tracking.

Glossary of terms	
Patellofemoral (PF) kinematics	Relative motion of the patella and femur (described by three rotations and 3 translations)
Patellar tracking	Measurement of the patella's location
Ex vivo	Studying cadaveric knees
In vivo	Studying living participants
In silico	Using computational methods

1.2. Patellar tracking methods

Patellar tracking shows the patellar alignment with respect to the femur during motion and thereby describes the six PF degrees of freedom (DOFs): three rotations and three translations (**Fig. 1**). Clinicians assess these PF kinematics by manual palpation of the patella during supine flexion-extension motions, while objective evaluation is done (1) *ex vivo* using cadaveric knees, (2) *in vivo* using living participants or (3) *in silico* (by computational modeling).

1.2.1. Ex vivo

Cadaveric studies allow the investigation of the contributions of specific structures, such as muscles or ligaments, on knee mechanics [17]. PF kinematics have been tracked for intact and ACL deficient knees [18] and under different artificially-induced loading conditions [19, 20]. Other studies implanted triads of markers on cadaveric patellae and mimicked *in vivo* knee activity by applying forces on the muscles crossing the knee [21] (**Fig. 2A**). An obvious limitation of *ex vivo* studies is that physiologically realistic conditions are not investigated, despite being the most clinically relevant to study.

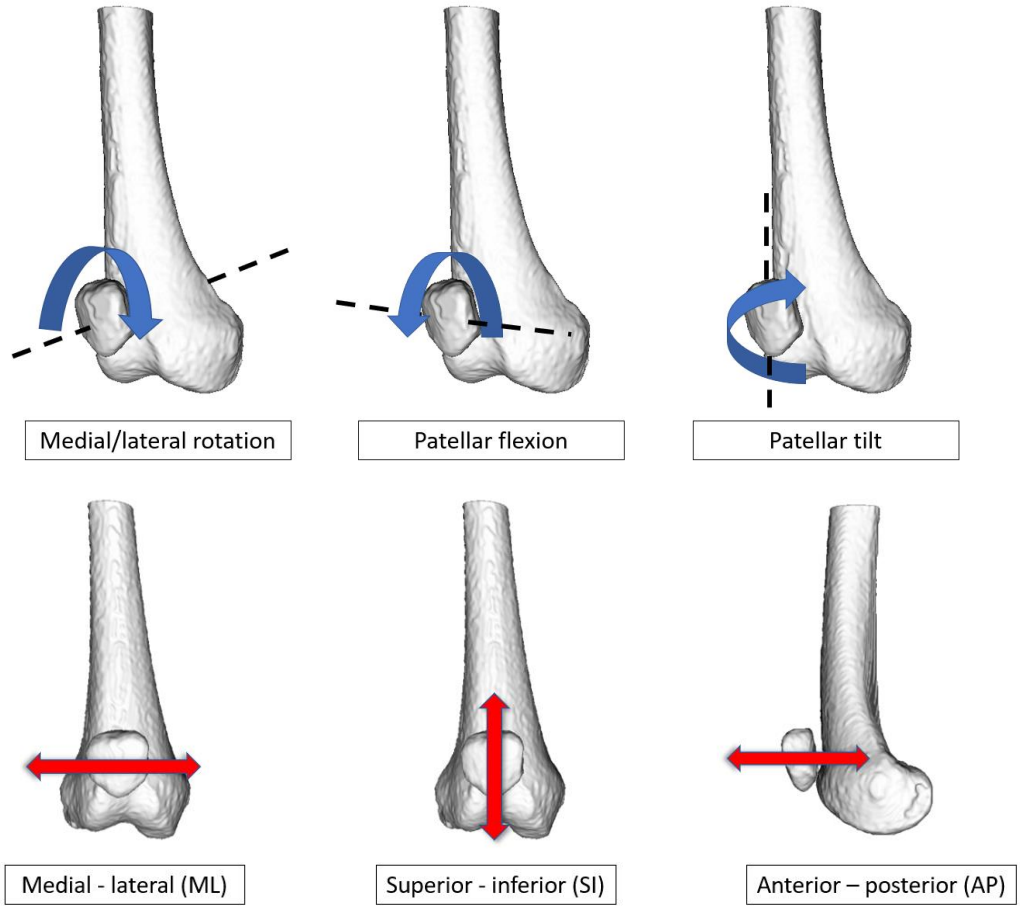

Fig. 1. The six degrees of freedom of the patellofemoral joint: the upper row shows the three rotations (blue arrows rotating around the black striped lines that represent the rotational axes) and the lower row shows the three translational degrees of freedom (red arrows).

1.2.2. In vivo

In vivo studies use optical motion capture, medical imaging techniques or both. The advantage of using living participants is that physiologically realistic conditions can be examined.

Optical motion capture is the non-invasive de facto standard for gait analysis and involves placement of retroreflective markers on the skin. Stereophotogrammetric cameras track the markers and these trajectories are used to describe the kinematics of bony segments from which joint kinematics are derived. Previous studies used optical motion capture to evaluate the tibiofemoral joint [22, 23], but few attempts have been made to do this for the patella. This is challenging due to the large relative motion of the skin over the underlying patella, also referred to as soft-tissue artefact (STA). STA is considerable for the patella: relative motions between the skin and patella of up to 40 mm have been found during knee flexion [24]. Previous studies tried to overcome this problem by placing a custom-molded clamp made of thermoplastics with infrared markers on the patella [21, 25, 26]. The clamp was pushed onto the knee using elastic bandage. However, bracing has been shown to affect PF kinematics [27], which calls into the question the validity of such a clamp. In addition to that, this method was only used in non-weightbearing and it was only tested up to a 20° knee angle.

An approach to track the kinematics of joints with much STA has been described for the shoulder [28, 29]. In these studies, joint kinematics were measured by placing a grid of markers on the skin covering the scapula. Throughout the range of motion of the shoulder, different markers were selected as markers covering specific bony structures and thereby STA was reduced. For the patella, conventional motion capture methods using anatomical markers do not work due to the large STA. The grid-based approach could overcome this problem, but no attempts to apply it on the patella have been made yet.

The second type of *in vivo* measurement involves medical imaging techniques. Conventional X-ray imaging, Magnetic Resonance Imaging (MRI) and computed tomography (CT) have been used to measure PF alignment at different knee angles during static conditions [30], and extrapolated to infer kinematics, but are of limited use when studying dynamic situations. Recent developments in medical imaging enabled dynamic patellar tracking using dynamic MRI [31] and four-dimensional CT (4D-CT) [32], although only slow motions and supine measurement are possible for these methods, respectively. These problems would be solved by biplanar videoradiography (BVR), a technique in which radiographic videos are taken simultaneously by two x-ray sources (**Fig. 2B**). Static 3D images of the bones (i.e. from a high resolution MRI) are then registered to the dynamic 2D scans in two planes based on the bone geometries. This has been done for the tibiofemoral joint [33, 34, 35], but is challenging for the patella due to its few morphological features [36]. In an attempt to still track the patella, some studies implanted radio-opaque markers or intracortical pins into the bone [21, 37]. This is very accurate but highly

invasive and therefore not suited for clinical use. In addition to that, studies using BVR require expensive equipment and no commercially available experimental setup exists yet.

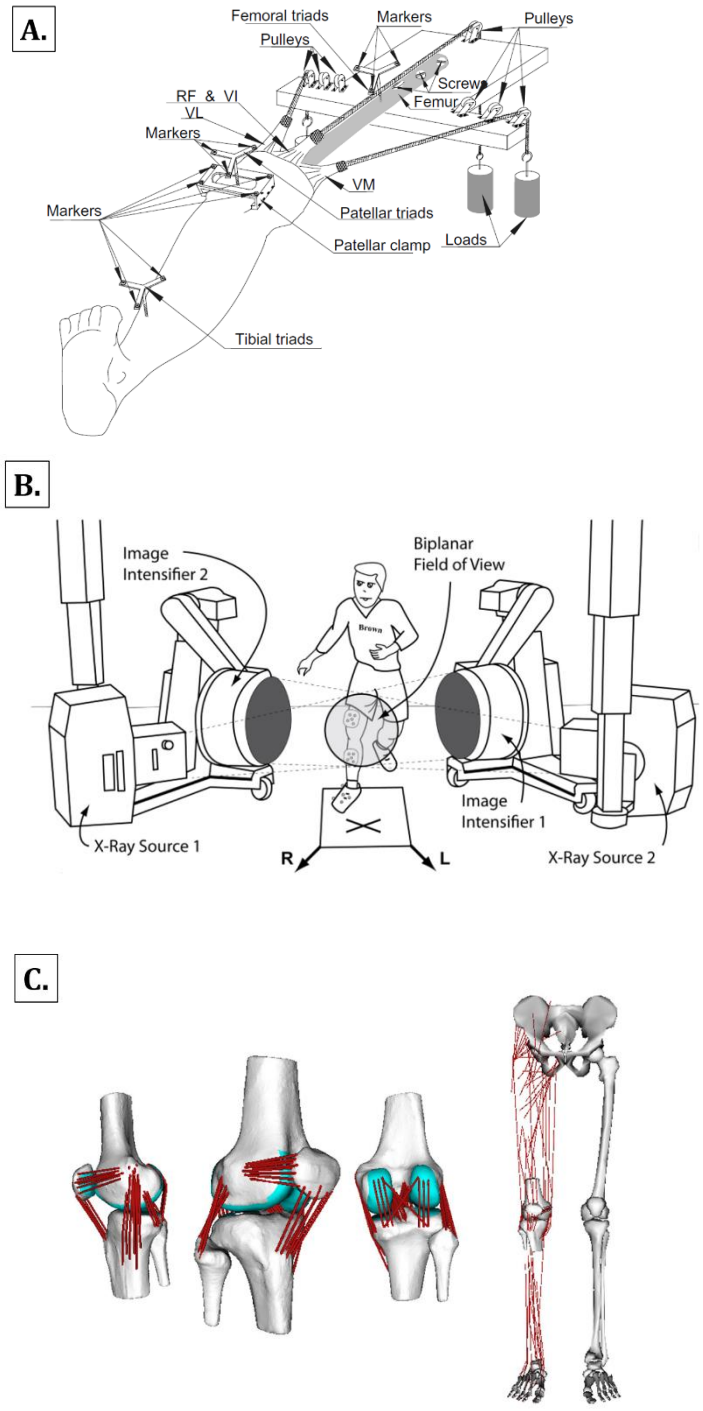

Fig. 2. Methods used to track PF kinematics. **A.** An in vitro study *[33]* in which optical motion capture was used to track marker triads that were implanted on the femur, patella and tibia of cadaveric knees. Muscle activity was simulated by loads applied to the rectus femoris (RF), vastus intermedius (VI) and vastus lateralis (VL). **B.** Experimental setup of biplanar videoradiography in which two x-ray sources are directed to the knee. Image intensifiers receive the x-rays and static CT-scans of the bones are registered onto the resulting videoradiographs in two planes *[34]*. **C.** A musculoskeletal model with bones, muscles and ligaments *[15]*. PF kinematics are simulated based on skin-mounted markers and ground reaction forces.

1.2.3. In silico

Computational models use optical motion capture, medical imaging data, or a combination of both to simulate the interplay of bones, muscles, and ligaments. Combined with force plate data, computational modeling enables the estimation of joint loads and stresses during motion. In addition to quantifying motions and forces, they can also be used to predict the effects of rehabilitation strategies and surgical outcomes by virtually applying different loading conditions at different muscle insertion sites. Computational models consist of elements that are used to estimate joint stress and pressure occurring at the article cartilage surfaces (e.g. finite element (FE) method, elastic foundation) and musculoskeletal models that quantify motion (i.e. inverse kinematics) or estimate loads and motions (i.e. forward dynamics) based on marker input.

Finite element models use MRI or CT scans to create knee models consisting of subject-specific bone- and cartilage geometries. Joint forces and stresses are then predicted based on cartilage deformation, which is a result of joint kinematics, muscles forces and external forces. The resulting PF joint forces then contribute to the simulated motion of the patella. Previous studies used FE models to estimate PF joint cartilage stress in healthy knees [38], in ACL deficient knees [39] and knees of individuals with PFP [10, 40]. A limitation of these models is that they are computationally intensive and especially difficult to solve for multi-body models (i.e. models representing the entire body or a complete leg) [13].

The other part of *in silico* methods involve musculoskeletal modeling. It assumes all bones are rigid and uses motion capture data to simulate multi-body models consisting of bones, muscles and ligaments. OpenSim is an open-source software program used to execute these simulations [41] and it consists of different knee models. We can divide these knee models into those without a patella [41, 42], models in which patellar motion is fully dependent on tibiofemoral knee flexion [43, 44] and models where all six DOFs of the patella are described [15, 45] (**Fig. 2C**). This last type of model is attractive as it better allows us to study pathological or diverging patellofemoral motion. Tibiofemoral kinematics, ground reaction forces, optimized muscle activity patterns and ligament properties are used to estimate the PF kinematics by these models. However, no experimental data relating directly to participant-specific patellar motion are used because no marker-based method to measure the patellar motion exists.

1.3. Problem definition

Determination of *in vivo* PF translations is done using medical imaging techniques or by (marker-based) musculoskeletal modeling, but these approaches have limitations.

Medical imaging: Dynamic MRI and 4D-CT only allow measurement of slow motions or supine conditions. Biplanar videoradiography enables measurement during functional upright motions

such as gait, but is less suitable for patellar tracking and requires expensive equipment, making it unavailable for many researchers and clinicians.

Musculoskeletal modeling: Most marker-based musculoskeletal models predict PF kinematics based on marker data describing tibiofemoral knee flexion with no specific inputs relating directly to participant-specific patellar motion. This makes it impossible to study pathological or deviating PF kinematics as no experimental data about the actual patellar location are used.

1.4. Study objective

The objective of this study was to develop a method designed to measure PF translations using optical motion capture by placing a grid of skin-mounted markers on the knee. The resulting patella identification algorithm was applied to two different types of data (4D-CT and optical motion capture) and compared to two existing methods (bone geometry-based and musculoskeletal model-based). We approached our objective by first answering our primary research question:

1. How well do CT-based PF translations obtained using a marker grid agree to those obtained using CT bone geometry-based coordinate systems?

To confirm the reliability of using our marker grid of two different measurements conditions and to compare our grid-based results to those obtained using a state-of-the-art musculoskeletal model, we aimed to answer two secondary research questions:

2. How do marker grid-based PF translations obtained using 4D-CT data compare to grid-based results obtained during optical motion capture?
3. When only using optical motion capture data, what is the difference between marker grid-based and musculoskeletal model-based PF translations?

This study is clinically relevant because a proof of concept could demonstrate the potential of a new, reliable method to measure PF translations. This method could serve as an alternative for expensive imaging techniques and could provide complementary kinematic information as marker input for musculoskeletal models used to study the PF joint.

2. Methods

One female (S01, age = 26 years, height = 163 cm, weight = 68 kg) and one male (S02, age = 27 years, height = 180 cm, weight = 81 kg) participant were recruited. Exclusion criteria were symptomatic PFP or PFOA. S02 had undergone an ACL reconstruction > 10 years prior to measurement. Ethical approval was given by the Medical Ethical Committee of Erasmus MC (Rotterdam, the Netherlands) and Human Research Ethical Committee (TU Delft, the Netherlands). Both participants signed an informed consent form approved by these institutions.

2.1. Data collection

Two types of measurements were conducted: (1) 4D-CT scanning and (2) optical motion capture. To identify the patella's location during motion, a grid of 42 retroreflective markers (Ø 3 mm) was placed on one knee at both measurements (**Fig. 3**). This number was chosen to ensure that the patella was covered during the entire range of motion of the knee. Prior to marker placement, the base, apex and the lateral and medial sides of the patella were palpated while participants were standing upright. These four palpated locations were then used to identify the remaining 38 marker locations by ensuring a distance of approximately 2 cm between each marker. We then drew these locations on the skin with a pen, which also enabled similar marker placement at both measurements.

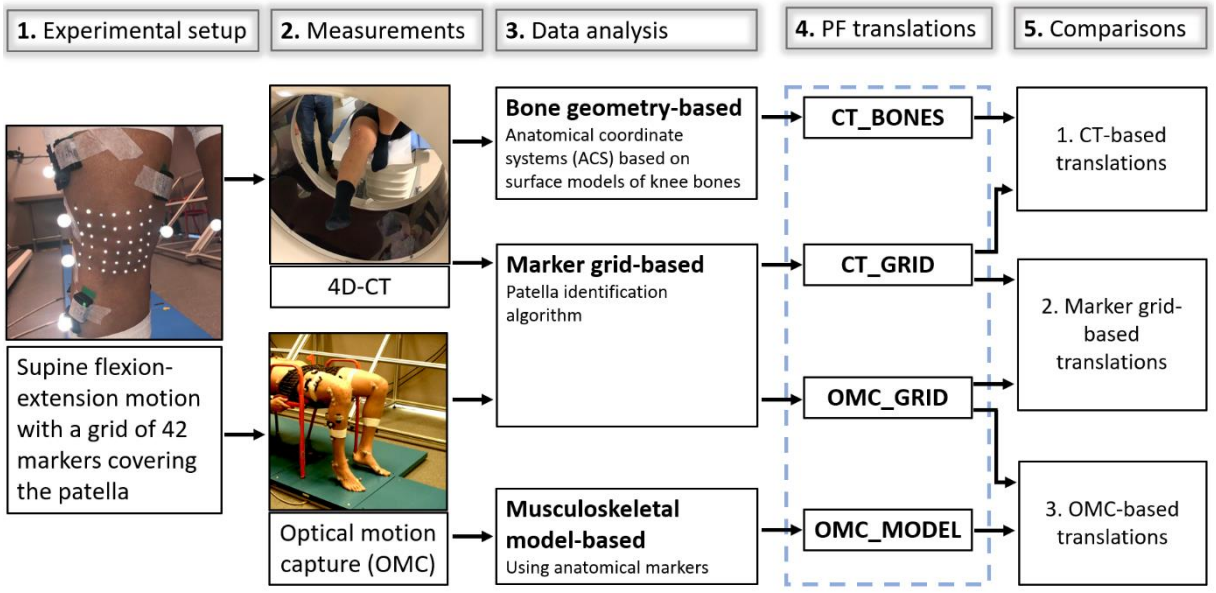

Fig. 3. Flow diagram describing the steps taken by this study. The dashed blue line shows the four different methods used to calculate the PF translations.

2.1.1. 4D-CT measurement

CT images were acquired using a 4D-CT scanner (TSX-301A-Aquilion ONE, Canon Medical Systems, Otawara, Japan). Prior to scanning, the marker grid was placed on the anterior knee surface, and three anatomical markers were placed on the femoral epicondyles and lateral tibia plateau, respectively. An experienced orthopedic surgeon assisted with the localization of these anatomical landmarks. First, a static 3D-CT scan of the extended knee was made while the participants were placed supine in the scanner to obtain sufficient geometrical information of the femur and the tibia to enable anatomical coordinate system determination (3D-CT properties: 1 mm slice thickness, 512 × 512 × 392 cubic voxels with 0.8 mm increment spacing, 40 cm capture volume in the longitudinal axis).

Next, participants were instructed to extend their knees from maximal allowed knee flexion to maximal extension in 10 seconds. The CT scanner allowed knee flexion up to approximately 50°. Dynamic 4D-CT scans were made during this motion at a sample rate of 2 Hz (0.5 mm slice thickness, 512 × 512 × 160 cubic voxels with 0.5 mm increment spacing, 16 cm capture volume in the longitudinal axis). Participants were trained to perform the motion with an instructor beforehand, using a metronome to guide movement speed. These measurements resulted in one static (3D) and 21 dynamic (4D) CT scans of the knee. Note that these 21 dynamic scans described the knee during one single flexion-extension motion. Radiation exposure for static and dynamic CT scans was 0.089 mSv and 0.39 mSv, respectively. Due to logistic problems, CT data of only one participant (S01) was available and used to evaluate the feasibility of using our grid-based method.

2.1.2. Optical motion capture

Marker trajectories were recorded using the Qualisys 3D motion capture system (Qualisys AB, Göteborg, Sweden), consisting of 12 stereophotogrammetric cameras. After the marker grid was placed on the patella, 26 additional markers (Ø 12 mm) were placed on anatomical landmarks of the legs, feet and torso, and 14 markers (Ø 12 mm) on 4 rigid plates were placed as marker clusters on the thighs and shanks. Identical to the 4D-CT measurements, participants performed a supine knee flexion-extension in the gait laboratory. This dynamic trial and one static trial were measured at a sample rate of 100 Hz. Motion capture was performed in the BioMechaMotion Lab at Delft University of Technology.

2.2. Data analysis

2.2.1. Patella identification algorithm

The marker grid trajectories obtained by 4D-CT and optical motion capture were used as input for the algorithm, which utilizes the fact that the patella protrudes from the knee anteriorly. During knee motion, the patella moves relative to the skin and therefore also relative to the skin-

mounted marker grid. This is why different markers were identified as markers covering the patella throughout an entire flexion-extension trial. The patella identification algorithm was created in MATLAB (Mathworks, Natik, MA, USA) and consists of four steps to calculate PF translations:

1. **Grid reference frame**: A marker grid reference frame was defined, based on three corner markers, with the Z-axis pointing anteriorly (**Fig. 4A**).
2. **Surface fitting**: The algorithm initially detected the five most anteriorly positioned markers and labelled them as markers covering the patella. The patellar centroid was then calculated by taking the mean position of these five markers. This, however, resulted in large jumps in the identified PF translations as the knee moved because of the considerable distance between the markers of approximately 20 mm. To solve this, cubic spline interpolation of the marker grid created third-order polynomials that constructed a smooth surface function going through all 42 markers (**Fig. 4B**). This surface function was then converted into 9000 virtual markers (**Fig. 4C**). This number was chosen to create smooth PF translations while limiting the algorithm's calculation time (< 15 seconds).

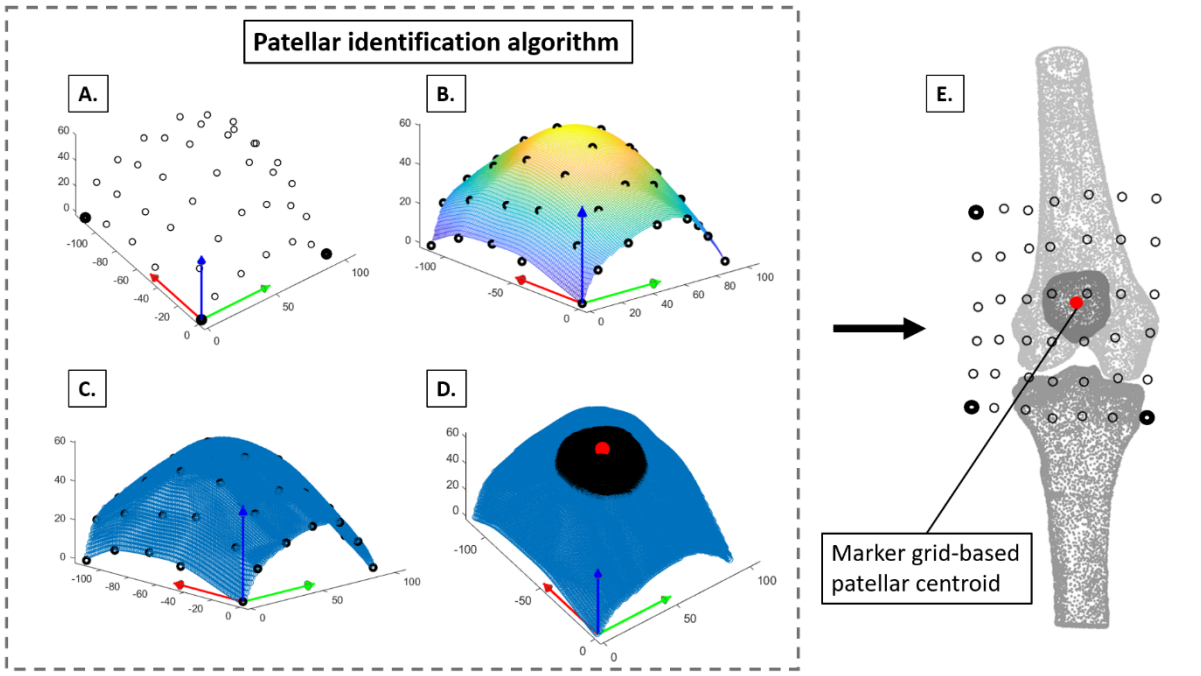

Fig. 4. A step-by-step description of the patella identification algorithm, in which PF translations are determined based on marker grid data. **A.** The marker grid reference frame generated based on three corner markers (bold). The axis vectors point in the medial (green), superior (red) and anterior (blue) directions. **B.** A surface function (colored) fitted through the 42 markers (black) using cubic spline interpolation. **C.** Virtual (blue) and real (black) markers. **D.** Identified patella region (black) and patellar centroid (red). **E.** A frontal view of the knee bones (grey), the marker grid (black), the corner markers (bold black) and the identified patellar centroid (red).

3. **Patella identification**: The 2000 virtual markers with the largest positive Z-value relative to the grid reference frame were selected as virtual markers covering the patella and these 2000 markers were used to identify the patellar location. This number was chosen such that the identified patellar dimensions were similar to those of the actual patella, which we obtained from CT images of the knee. This virtual marker selection represented the grid-based patellar location, and the mean coordinate of this region defined the centroid of the patella (**Fig. 4D**).
4. **Knee angle calculation**: For the 4D-CT data sets, bone geometries were used to determine femoral and tibial coordinate systems [46], which were then used to calculate the knee angle (this will be explained in more detail in the next section). For optical motion capture, the femoral coordinate system was constructed using the markers placed at the medial and lateral epicondyles and the anterior superior iliac spine (ASIS) and had its origin at the center of the epicondyles. The tibial coordinate system was constructed using the markers placed at the lateral tibia plateau and the medial and lateral malleoli and had its origin at the center of the malleoli. The longitudinal axes of both bones defined the knee angle, which was based on the work of Grood and Suntay [47].

Finally, the location of the patellar centroid (estimated by the patella identification algorithm) relative to the femoral coordinate system was described in terms of three PF translations: medial – lateral (ML), superior – inferior (SI) and anterior – posterior (AP). Calculated translations were described as a function of knee angle.

2.2.2. 4D-CT: segmentation, registration and patellar tracking

We evaluated the feasibility of our new, grid-based method by comparing its results (i.e. the PF translations) to those obtained using 4D-CT images describing the bone geometries of the femur, patella and tibia. First, one static (3D) and 21 dynamic (4D) CT scans were segmented using 3D Slicer (version 4.11) [48]. Three-dimensional surface models of the bones were automatically identified based on image pixel intensity and smoothed (<0.1 mm deviation from original model). We also created surface models of the marker grid by manually creating 3D spheres at all 42 grid marker locations (**Fig. 5A-D**).

The segmented dynamic bone models had the correct position and orientation (pose) with respect to each other but, due to limited field of view during data collection, the amount of visible femur and tibia was not enough to provide sufficient geometric information to accurately calculate the femoral and tibial coordinate systems. The static surface models of these two bones were therefore registered onto the dynamic surface models, since the static images were of a larger field of view. We performed rigid bone model registration by applying an iterative closest point (ICP) algorithm to the surface models using the Python package Trimesh. The static femur and tibia models were translated and rotated until they fit onto the short, dynamic bone models (**Fig. 5E**).

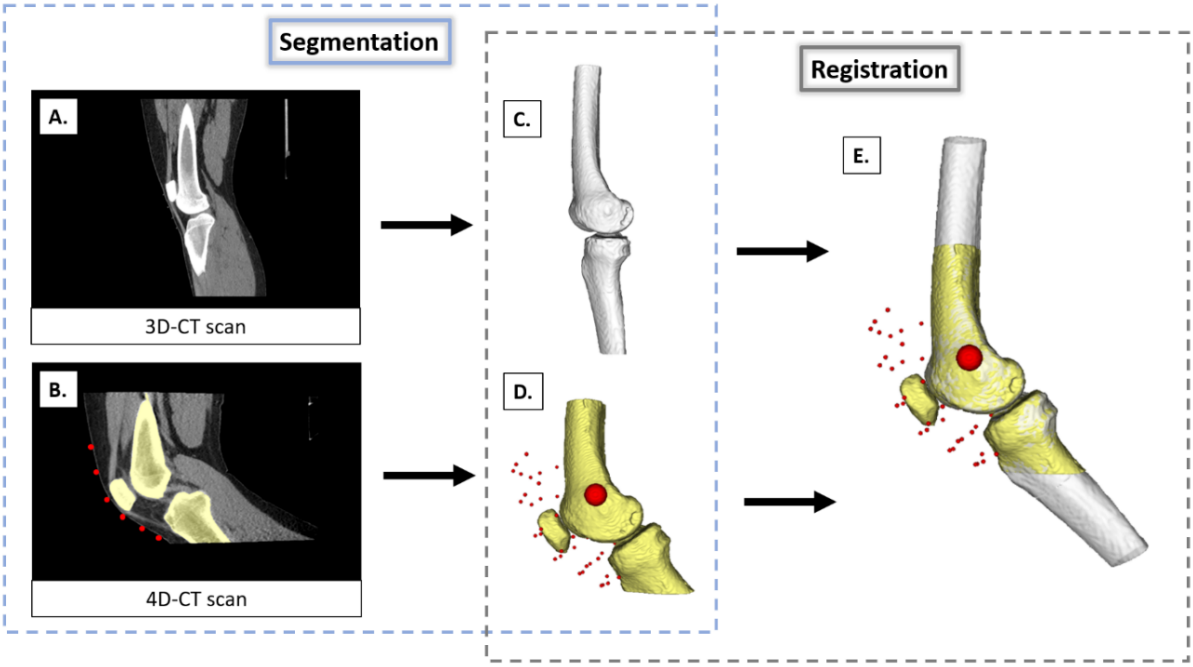

Fig. 5. The segmentation and registration of CT data. **A.** Sagittal view of a static CT scan of an extended knee. **B.** Sagittal view of a dynamic CT scan of the knee during knee flexion showing the bones (yellow) and marker grid (red). **C.** Surface model of the static femur and tibia used for registration **D.** Surface models of the dynamic femur, patella, tibia and marker grid. **E.** Completed registration. The resulting surface models of the femur, patella and tibia were used to determine PF translations CT_BONES. The marker grid (red) was used to determine CT_GRID.

Post-processing of the registered bone models in Geomagic Wrap 2015 (Research Triangle, NC, USA) involved surface smoothing and node decimation to reduce computational time. The surface models of the femur, patella and tibia were decimated to 16000, 5000 and 7000 triangles, respectively. This eventually resulted in surface models of the femur, patella, tibia and marker grid for all 21 scans.

Next, we determined the anatomical coordinate systems (ACS) of the three bones and the PF joint kinematics. Bone geometries provided by the surface models were used to determine the ACS of the femur, patella and tibia using an morphology-based, automated method developed by Chen et al. [46]. Their method works well for 4D-CT data of the knee as it only requires geometric information of the distal femur and proximal tibia. This algorithm combined and improved existing methods developed for the femur and tibia [49] and the patella [50]. The three orthogonal axes of the femoral ACS were constructed by first fitting two cylinders through the femoral epicondyles. A line going through the center of these cylinders defined the medial-lateral axis and the midpoint of this line was selected as femoral origin. The remaining femoral axes were constructed using the diaphyseal inertial axis (superior – inferior axis) and by calculating the vector perpendicular to the aforementioned axes. The tibial ACS was created by determined using

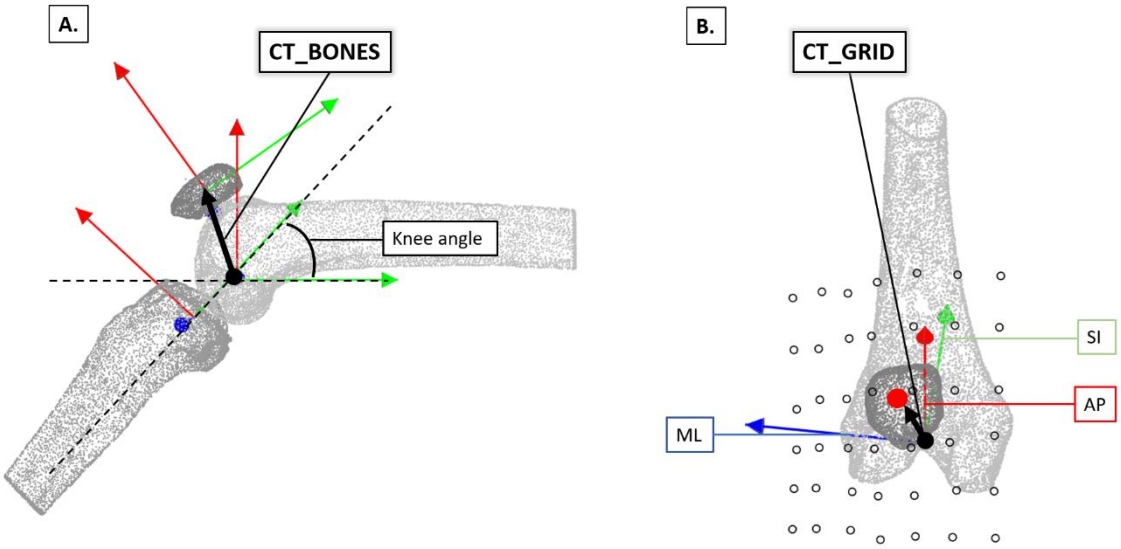

Fig. 6. Description of how surface models of the bones and marker grid are used to describe both CT-based PF translations. **A.** Sagittal view of the knee bones together with their bone geometry-based anatomical coordinate systems (ACS). First, the knee angle is defined by the femoral and tibial longitudinal axes. Then, bone geometry-based PF translations (CT_BONES, black arrow) are determined using the femoral and patellar ACS. **B.** Frontal view of the femur, patella, femoral ACS, marker grid and patellar centroid determined by the patella identification algorithm (red point). The marker grid-based PF translations (CT_GRID, black arrow) are given in each direction: medial-lateral (blue), superior-inferior (green) and anterior-posterior (red).

the inertial axis of the long shaft and the cross-sectional area in the longitudinal direction. The patellar ACS was constructed by first identifying the patellar ridge, base and apex and then creating the ACS axes based on these landmarks. The codes used to determine the ACSs can be found at https://github.com/BioMechTools/DKCT_Quatitative_Measurement. The resulting axes and origins of the bones were then used to calculate the knee angle and the bone geometry-based PF translations, respectively. We labelled these PF translations (mm) at different knee angles using the CT bone geometry-based approach as CT_BONES (**Fig. 6A**).

To evaluate our proof of concept, we calculated the patellar position derived from the patellar identification algorithm using the CT-based marker grid data for all 21 scans and compared these values to CT_BONES. The resulting patellar centroid described the dynamic behavior of the patella relative to the femur. We labelled these PF translations (mm) at different knee angles using CT-based marker grid data as CT_GRID (**Fig. 6B**).

A constant difference between CT_BONES and CT_GRID could indicate that both methods measured the same patellar motion, but described the trajectory of a different location of the patella. Therefore, differences in ML, SI and AP directions were calculated for each knee angle.

2.2.3. Optical motion analysis: marker-based methods

Two types of marker data sets were obtained using Qualisys Track Manager Software (QTM, version 2021.2). First, marker grid trajectories obtained during the flexion-extension trial were tracked and used as input for the patella identification algorithm we described previously. A

Gaussian-weighted moving average filter (smoothing factor 0.25) was applied to the resulting translations to reduce noise. This resulted in the PF translations (mm) at different knee angles which we labelled as OMC_GRID.

Next, we used the trajectories of anatomical markers to estimate patellar motion using a generic musculoskeletal model in OpenSim (**Fig. 7A**). This model, developed by Lenhart et al. [15], consists of 25 bones, 44 muscles and 14 ligaments. First, marker data of the static trial were used to scale the bones sizes and inertial properties [51]. This was done based on marker distances between anatomical markers (e.g. the distance between the ASIS and the lateral femoral epicondyle was used to scale the femur) (**Fig. 7B**). Then, PF translations were estimated using the anatomical marker trajectories obtained during the dynamic flexion-extension trial (**Fig. 7C**). It is important to note that, for this method, no marker grid data was used since we used an existing method to obtain PF translations. Tibiofemoral kinematics were determined using a global optimization inverse kinematics routine on the anatomical landmarks. Cartilage contact pressures at the tibiofemoral and patellofemoral joints were modelled using a non-linear elastic foundation model, a method in which cartilage pressure is assumed as a function of cartilage penetration depth [52]. Ligaments were represented as bundles of non-linear springs (elastic modulus of 125 MPa) and muscle activity was simulated using a modified computed muscle control algorithm [53]. This global optimization algorithm computed muscle excitations needed to achieve the calculated tibiofemoral kinematics. Finally, PF translations were estimated by forward dynamics, in which PF translations were a function of muscle and ligament forces and cartilage contact. A Gaussian-weighted moving average filter (smoothing factor 0.25) was applied to the resulting translations to reduce noise. The resulting PF translations (mm) at different knee angles were labelled as OMC_MODEL.

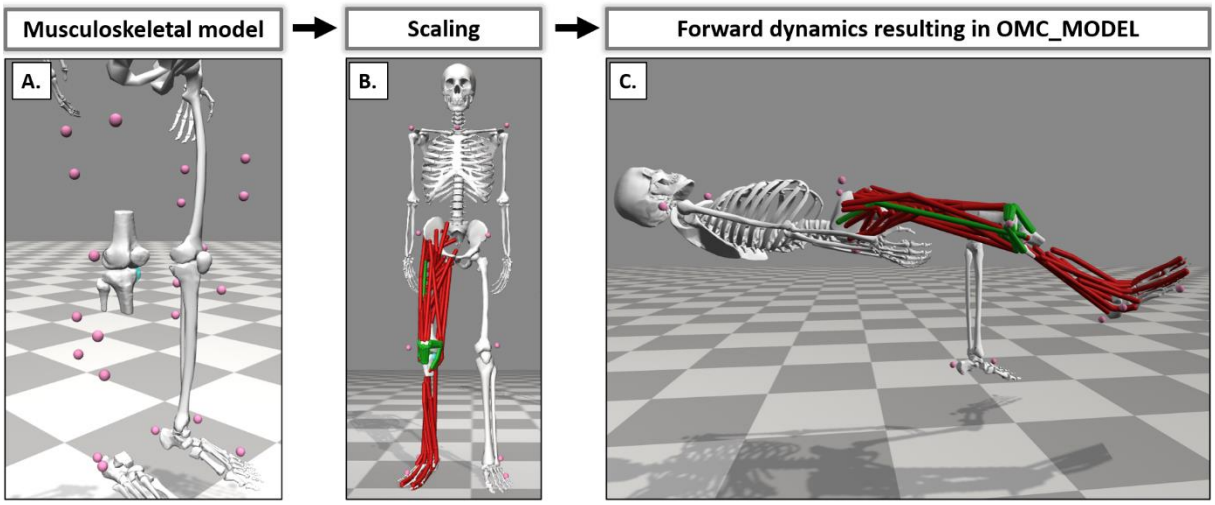

Fig. 7. A. The generic musculoskeletal model and anatomical markers used to calculate the OMC_MODEL. The creators of this model only showed the distal femur, and proximal tibia. **B.** Scaled model with 44 muscles (red) and 14 ligaments (green). **C.** The flexion-extension simulation performed using global optimization inverse kinematics, a modified computed muscle control algorithm and forward dynamics.

2.3. Methodological comparisons

We determined PF translations in four different ways: using a CT bone geometry-based approach (CT_BONES), using CT data describing a marker grid (CT_GRID), using optical motion capture of a marker grid (OMC_GRID) and using optical motion capture combined with musculoskeletal modeling (OMC_MODEL). Because these methods used different approaches, differences in initial PF translations (i.e. offset) were seen at the start of the trial. We set all PF translations to 0 mm at maximal knee flexion (i.e. the start of the trial) in order to eradicate any offset caused by the use of different methods. After this normalization, three comparisons were made.

First, to evaluate the proof of concept of our marker grid-based method, we first compared CT_GRID to CT_BONES. A second order polynomial was fitted through the 21 data points of both results. In addition to that, we analyzed the absolute error in each direction between CT_BONES and CT_GRID. This analysis was done by presenting the errors at each knee angle. Second, CT_GRID and OMC_GRID were compared to evaluate how well marker grid-based PF translations using two different methods of data acquisition (i.e. CT and OMC) agreed. Third, both methods using optical motion capture, OMC_GRID and OMC_MODEL, were compared to see how well our marker grid-based method performed relative to an existing, state-of-the-art anatomical marker-based musculoskeletal model.

The patella engages into the femoral trochlear groove around 20° knee flexion [54] and at knee angles below this point (< 20°) the patella lies proximal to the trochlear groove and it rests on the suprapatellar fat pad. This makes it difficult to measure the patellar location using skin-mounted markers because there is no bony protrusion (**Fig. 5A**). At knee angles above this point (> 20°), the patella lies within the trochlear groove, in other words there is 'patellar engagement'. Because of this, we analyzed PF translations for all knee angles (KA_ALL), but also for knee angles belonging to the patellar engagement phase (KA_ENGAGED, > 20°).

Finally, the excursion of the patella relative to the femur was determined in all three directions for each method. We then calculated differences in excursions between methods to see how well the ranges of motions agreed. For example, excursion in the ML direction described the distance between the most medial and most lateral position of the patella relative to the femur.

2.4. Statistical analysis

The Pearson correlation coefficient (*r*) and root mean square error (RMSE) of the difference were calculated for all three comparisons during KA_ALL and KA_ENGAGED using MATLAB. A correlation coefficient > .75 was considered as strong and > .5 as moderate [55]. To evaluate agreement between CT_BONES and CT_GRID (and thereby enabling us to answer our primary research question), a Bland-Altman plot was made for both KA_ALL and KA_ENGAGED.

3. Results

3.1. 4D-CT: bone geometry-based vs. marker grid

The CT-based PF translations CT_BONES and CT_GRID showed similar patterns, especially at knee angles larger than 20° (KA_ENGAGED) (**Fig. 8**). As the knee moved from maximal flexion (48°) to a 20° knee flexion, both methods predicted a patellar motion going superiorly, anteriorly followed by posteriorly, and making a C-shaped curve in the ML direction (starting laterally, translating medially and then returning laterally). At knee angles < 20° (i.e. more extended knee positions), CT_BONES and CT_GRID showed larger differences, especially in the SI direction. This is visualized by the errors between both results (**Fig. 9**). During KA_ENGAGED, the accumulative error was relatively constant (mean ± SD: 3 mm ± 2 mm) while below this region (knee angles < 20°), larger errors (especially in the SI direction) were seen. This translated to a larger total error in estimated PF translations (mean ± SD: 25 mm ± 7 mm), reaching its maximum of 31 mm at 4° knee flexion. Second order polynomials were fitted to both CT-based results. To remove the effect of the large error in SI direction below 20° knee flexion, a second order polynomial was fitted on CT_GRID data points within KA_ENGAGED only, resulting in more similar SI translations.

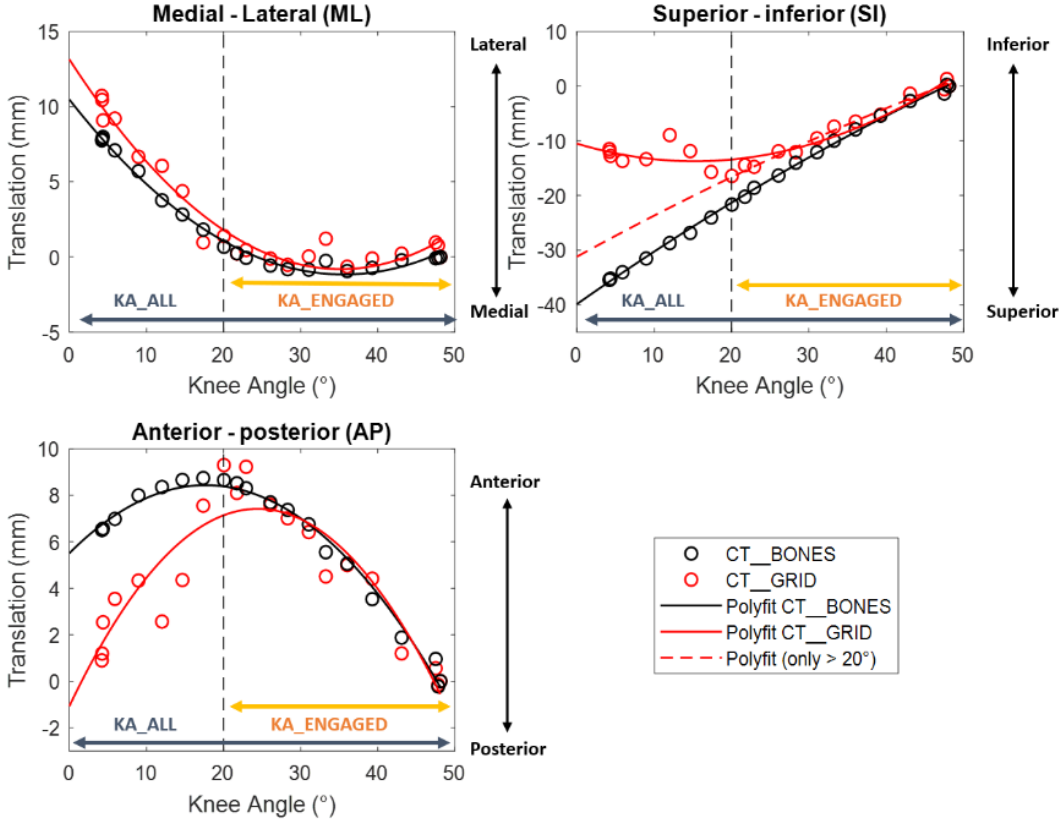

Fig. 8. Patellofemoral translations in all three directions at different knee angles for both CT-based methods for S01 during one trial. Dashed black vertical lines at 20° indicate the starting point of KA_ENGAGED. Solid lines represent 2nd order polynomials fitted through the data points of CT_BONES (black) and CT_GRID (red). The dashed red line in the SI direction represents the 2nd order polynomial fitted only on data points of CT_GRID within the knee angle range KA_ENGAGED.

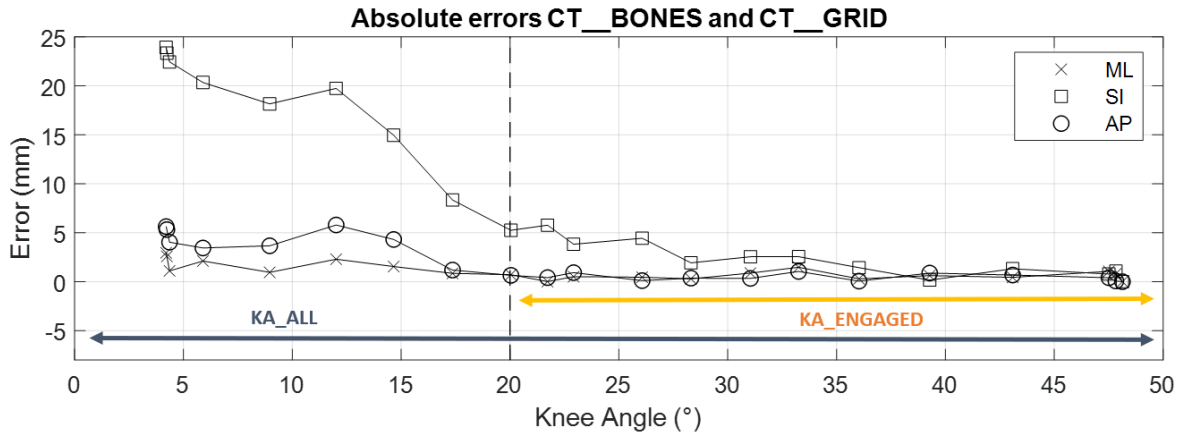

Fig. 9. Differences between CT_BONES and CT_GRID at different knee angles for S01 during one trial. Dashed black lines at 20° indicate the starting point of KA_ENGAGED.

Table 1. Patellar excursion (mm) in ML, SI and AP directions for both CT-based methods and for both knee angle ranges. The differences (mm) between the excursions describe how much the patellar ranges of motions between these methods differ.

	Excursion during KA_ALL (mm)			**Excursion during KA_ENGAGED (> 20°) (mm)**		
	ML	**SI**	**AP**	**ML**	**SI**	**AP**
CT_BONES	9	36	9	2	22	9
CT_GRID	11	18	9	2	18	9
Differences	**2**	**18**	**0**	**0**	**4**	**0**

Maximum differences in patellar excursion between CT_BONES and CT_GRID were larger for KA_ALL (18 mm) than for KA_ENGAGED (4 mm) (**Table 1**). The small differences seen at KA_ENGAGED indicate similar ranges of motion of the patella relative to the femur are estimated by both methods for knee angles > 20°.

3.2. Marker grid: 4D-CT vs. optical motion capture

Marker-grid based PF translations using 4D-CT data (CT_GRID) and optical motion capture (OMC_GRID) showed similar patterns during both KA_ALL and KA_ENGAGED (**Fig. 10**). However, the two methods start at a different tibiofemoral knee angle which results in a horizontal shift of approximately 10° in the graphs of all three PF translations. This shift is caused by the fact that different ways to calculate the knee angles are used: CT_GRID used anatomical coordinate systems based on bone geometries while OMC_GRID used anatomical markers placed on the hip (ASIS), knee and ankle. To allow comparison of results without the effect of selected knee angle definitions, this initial difference of 10° knee flexion was removed by applying a horizontal shift of 10° (**Fig. 10**: dashed blue line).

Analysis of the patellar excursions suggests that CT_GRID and OMC_GRID showed similar patellar ranges of motions relative to the femur (**Table 2**). Differences in the ML, SI and AP directions between both methods were 1 mm, 2 mm and 4 mm during KA_ALL and 5 mm, 1 mm and 2 mm during KA_ENGAGED. Visual inspection of the graphs describing the PF translations agree with this.

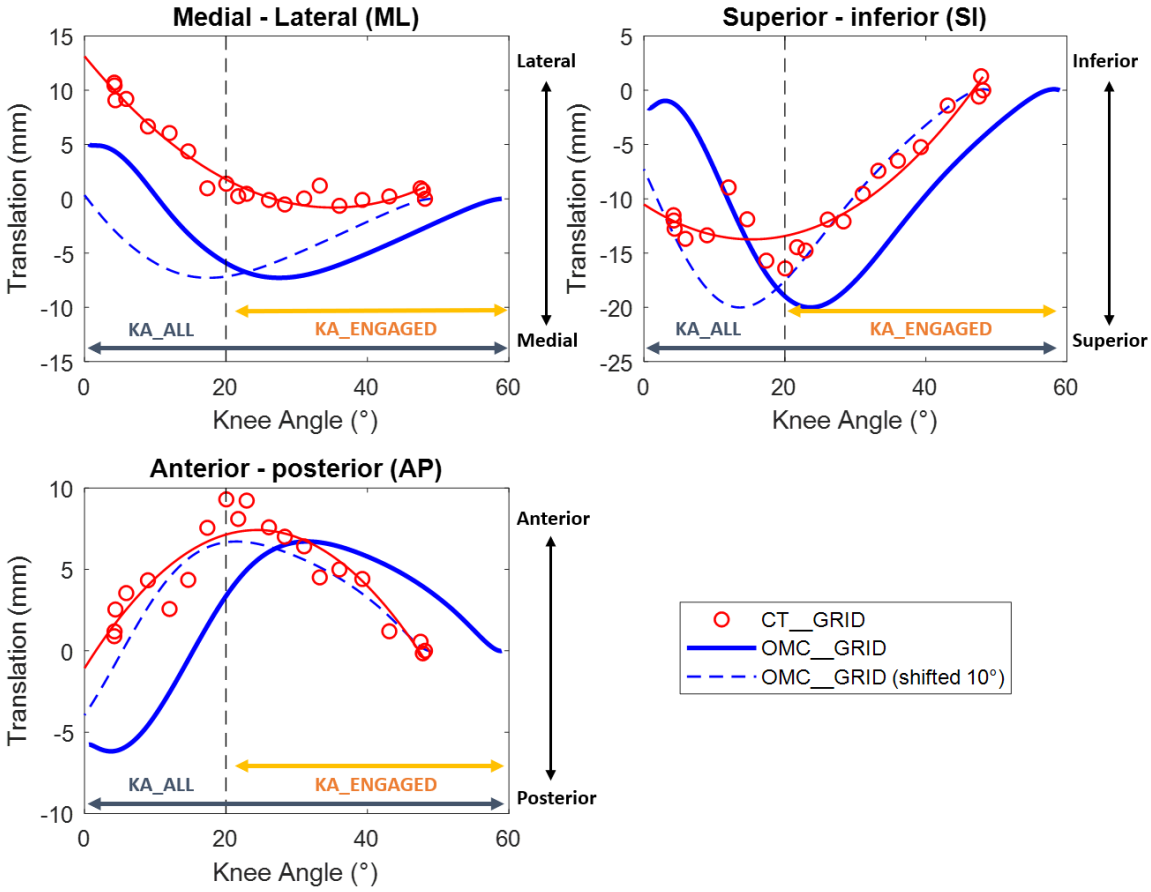

Fig. 10. Patellofemoral translations in all three directions at different knee angles for both marker grid-based methods. Dashed black vertical lines at 20° indicate the starting point of of KA_ENGAGED. The PF translations estimated by OMC_GRID are represented as original (solid blue) and after results are shifted horizontally by 10° (dashed blue).

Table 2. Patellar excursion (mm) in ML, SI and AP directions for both marker grid-based methods and for both knee angle ranges. The differences (mm) between the excursions describe how much the patellar ranges of motions between these methods differ.

	Excursion during KA_ALL (mm)			**Excursion during KA_ENGAGED (> 20°) (mm)**		
	ML	**SI**	**AP**	**ML**	**SI**	**AP**
CT_GRID	11	18	9	2	18	9
OMC_GRID	12	20	13	7	17	7
Difference	**1**	**2**	**4**	**5**	**1**	**2**

3.3. Optical motion capture: marker grid vs. musculoskeletal modeling

Optical motion capture-based PF translations estimated using a marker grid (OMC_GRID) and musculoskeletal model simulation (OMC_MODEL) were similar in the SI directions but different in the ML and AP directions (**Fig. 11**). In the SI and AP directions, differences in peak-to-peak displacement were smaller for KA_ENGAGED (< 7 mm) than for KA_ALL (< 10 mm). In the ML direction, the difference was larger for KA_ENGAGED. PF translations estimated by OMC_MODEL were only provided by the simulation for knee angles > 12°. Note that, while previous (CT-based) comparisons only evaluated S01, the current comparison involved data of both participants.

Peak-to-peak displacements for OMC_GRID and OMC_MODEL were similar in the SI direction for both KA_ALL and KA_ENGAGES (differences of 3 mm and 0 mm, respectively), but less in the ML and AP directions (**Table 3**). This agrees with visual inspection of these graphs (**Fig. 11**), considering OMC_MODEL showed a 16 mm larger lateral motion at 20° and completely different shapes are observed in the AP direction.

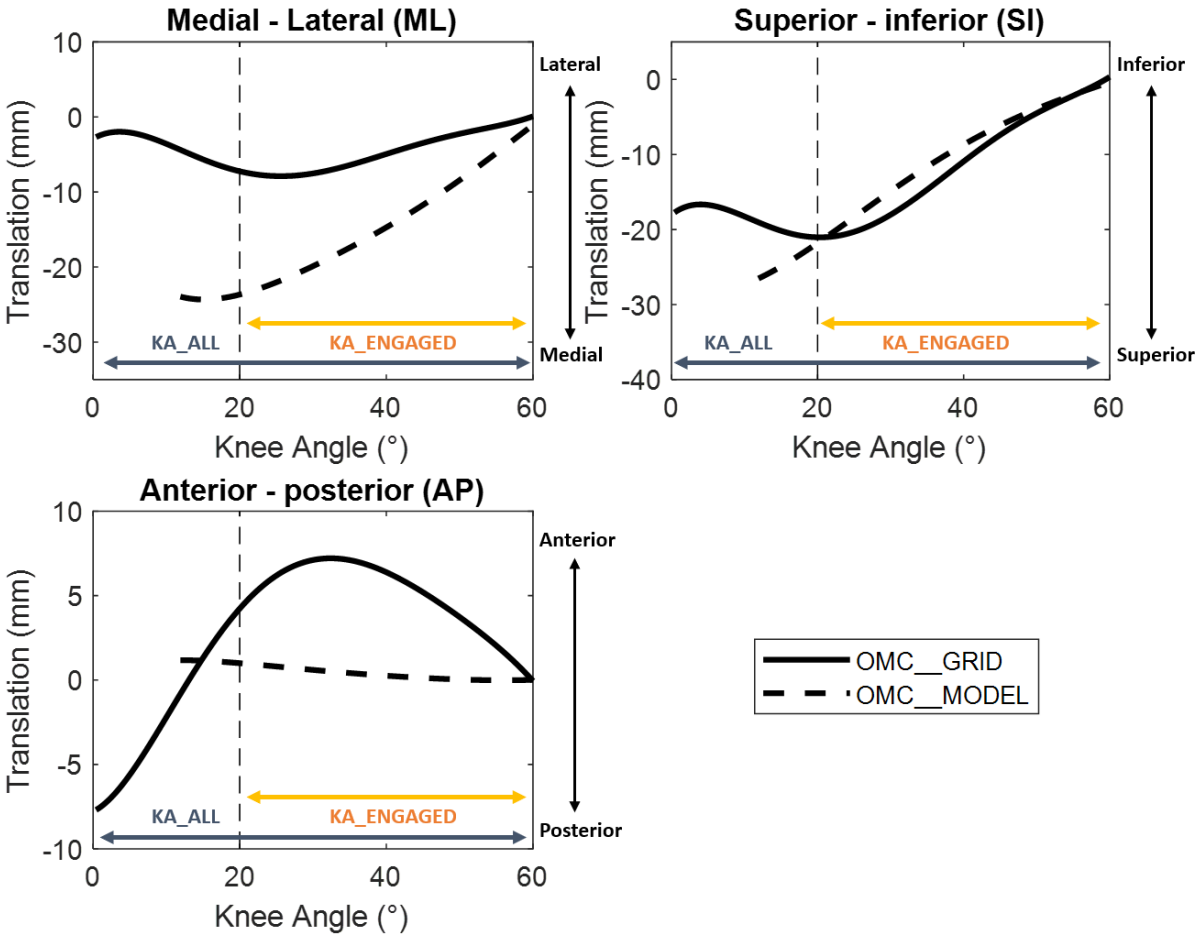

Fig. 11. Patellofemoral translations in all three directions at different knee angles for both optical motion capture-based methods. Dashed black vertical lines at 20° indicate the starting point of of KA_ENGAGED.

Table 3. Peak-to-peak patellar displacement (mm) in ML, SI and AP for both methods using optical motion capture. Displacements are determined for both knee angle ranges.

	KA_ALL			KA_ENGAGED (> 20°)		
	ML	**SI**	**AP**	**ML**	**SI**	**AP**
OMC_GRID	5	26	12	5	22	8
OMC_MODEL	25	29	2	24	22	1
Difference	**20**	**3**	**10**	**19**	**0**	**7**

3.4. Statistical analysis

The outcomes of the statistical analyses are presented in **Table 4.** Pearson's correlation coefficients (*r*) between CT_BONES and CT_GRID were moderate to strong during both knee angle ranges in all directions, but stronger for KA_ENGAGED. Larger maximum RMSEs were observed during KA_ALL (12 mm) compared to KA_ENGAGED (3 mm), indicating smaller differences between CT_BONES and CT_GRID were seen for knee angles > 20° (compared to KA_ALL).

For the comparison of both grid-based results CT_GRID and OMC_GRID, no correlation was seen in the ML direction, while strong correlations were seen in the SI and AP directions during both KA_ALL and KA_ENGAGED. These correlations were stronger ($r > .97$) during KA_ENGAGED. This is in line with observation that the RMSEs during KA_ALL and KA_ENGAGED in the ML direction were 8 mm and 5 mm, respectively, while those in the SI and AP directions did not exceed 3 mm. In all directions, RMSEs were lower during KA_ENGAGED compared to KA_ALL.

Finally, strong correlations were seen between OMC_GRID and OMC_MODEL in the SI direction for both knee angle ranges ($r > .95$). Consistent with visual inspection of both results in the AP direction, no correlation was observed during. RMSEs were similar during KA_ALL and KA_ENGAGED in all directions and relatively large in the ML direction (12 mm and 10 mm, respectively).

We finally performed the Bland-Altman analysis for both knee ranges to evaluate how much CT_BONES and CT_GRID agreed (**Fig. 12**). For both KA_ALL and KA_ENGAGED, all data points were located within the upper and lower limits of agreement. The distance between the two lines of agreement determine how well the two results (CT_BONES and CT_GRID) agree. The distance of these regions during KA_ALL were 4 mm, 35 mm and 9 mm (ML, SI and AP, respectively), while those during KA_ENGAGED were only 2 mm, 8 mm and mm. This shows a better agreement during KA_ENGAGED, especially when looking in the ML and AP direction.

Table 4. Statistical outcomes. Pearson's correlation coefficients (*r*) and root squared mean of the error (RSME) for all comparisons.

Analysis	Methods	KA_ALL			KA_ENGAGED (> 20°)		
		ML	SI	AP	ML	SI	AP
r	CT_BONES vs. CT_GRID	.98	.78	.71	.76	.99	.98
	CT_GRID vs. OMC_GRID	.00	.91	.89	.00	.99	.97
	OMC_GRID vs. OMC_MODEL	.55	.97	.00	.51	.99	.00
RMSE (mm)	CT_BONES vs. CT_GRID	1	12	3	1	3	1
	CT_GRID vs. OMC_GRID	8	3	2	5	1	1
	OMC_GRID vs. OMC_MODEL	12	3	5	10	2	5

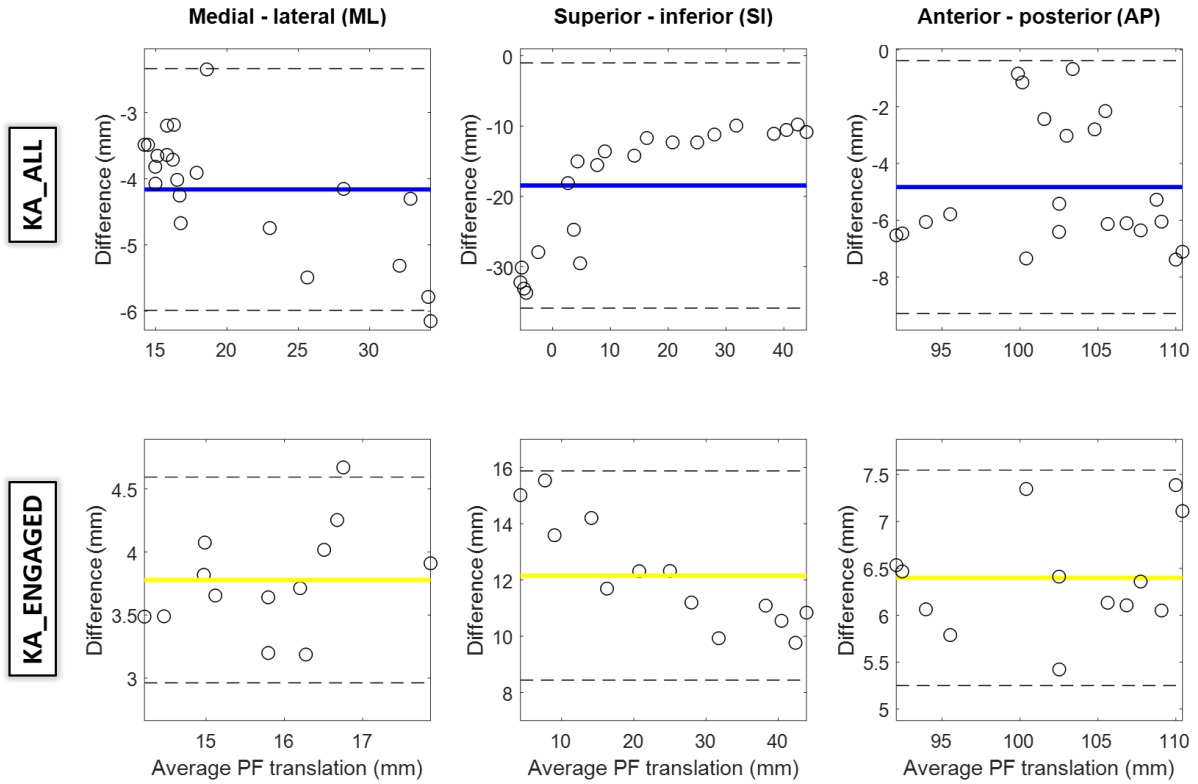

Fig, 12. Bland-Altman plots showing agreement between CT_BONES and CT_GRID during KA_ALL (upper row) and KA_ENGAGED (lower row).

4. Discussion

We introduced a marker grid-based method designed to non-invasively track *in vivo* patellofemoral translations and demonstrated a proof of concept. To our knowledge, this study is the first to assess these PF translations using skin-mounted markers placed on the knee. Comparison with the current gold standard (i.e. 4D-CT) showed promising results and suggests that this new method could serve as an alternative for expensive imaging techniques and could provide complementary kinematic information as marker input for existing musculoskeletal models used to study the PF joint.

Comparing the marker grid-based method to 4D-CT images

We first evaluated PF translations estimated by our marker grid-based method (CT_GRID) together with the bone geometry-based results (CT_BONES), which is considered to be a gold standard [32]. The results were promising for knee angles > 20° (KA_ENGAGED), considering similar PF translations were found by both CT-based methods (**Fig. 8**). Moderate to strong correlations between both results were seen and these were even stronger during KA_ENGAGED. This agrees with the maximal RMSEs found between both CT-based results. These findings demonstrate that it is possible to measure PF translations using a marker grid.

A problem occurred at knee angles < 20°, namely larger errors between CT_BONES and CT_GRID are observed (**Fig. 9**). The largest contribution to this error is seen in the SI direction, which reaches 23 mm and accounts for 97% of the total error at 4° knee flexion. These larger errors can be explained by the fact that the patella is not engaged with the femoral trochlea and it rests on the suprapatellar fat pad at knee angles < 20°. Within this range of knee angles, the patella is not pushed anteriorly by the femoral condyles anymore and the bone does, therefore, not protrude from the knee (**Fig. 5A**) [54]. That said, individuals suffering from PF pathologies (i.e. PFOA, PFP) experience most pain during flexed knee angles, for example when standing up from a chair or during running [56]. Therefore, the proof of concept given by this study is a valuable first step in improving research on these PF pathologies.

4D-CT vs. optical motion capture

The second comparison visualized how well grid-based PF translations agreed when using different methods of acquiring the data (i.e. 4D-CT and optical motion capture). Visual inspection and differences in patellar excursion suggest that CT_GRID and OMC_GRID predicted similar PF translations in the SI and AP directions. Strong correlations during both knee angle ranges confirm this finding, although no correlation was seen in the ML direction. This agrees with the large RMSE seen in the ML direction (8 mm), while those in the other two directions were considerably smaller (< 3 mm and < 1 mm during KA_ALL and KA_ENGAGED, respectively).

The large differences in the ML direction are unexpected. We placed the marker grid nearly identical during both measurement types and therefore expected a nearly perfect agreement between CT_GRID and OMC_GRID. A potential explanation for the large error in the ML direction is that data sets belonging to two different trials were used. Although similar motions were performed by the participant during CT and OMC measurement, it is possible that these different circumstances during measurement resulted in different PF kinematics. Another possible cause for the ML error could be that different femoral coordinate systems were used to describe the patellar motion relative to by both methods. CT_BONES used a the morphology of the femur, while

CT_GRID used a femoral coordinate system based on markers placed on the ASIS and femoral epicondyles, which could introduce STA of the anatomical markers.

This could also explain the fact that both results had similar shapes but a horizontal shift of 10° was seen at OMC_GRID in all three directions (**Fig. 10**). When using the greater trochanter instead of the ASIS to determine the femoral coordinate system, this was found to differ by approximately 10°. To enable better comparison, we therefore tried to remove the effect of knee angle definition by shifting OMC_GRID by 10°. This won't be needed for future research in which marker-based patellar location is used for existing musculoskeletal simulations, considering the same anatomical markers are used to determine the femoral coordinate system.

Comparison with musculoskeletal model simulations and the literature

To see how our findings agree with those found in the literature, the results of our method (OMC_GRID) were first compared to those estimated by an existing marker-based musculoskeletal model (OMC_MODEL). Strong correlations and small RMSEs were seen in the ML and SI directions, whereas results agreed considerably less in the AP direction. This could be caused by the fact that the musculoskeletal model used bone surface models of another participant, which means different bone geometries of the femur and patella were used for simulation. The differences in results could also be a result of the fact that no experimental data was used by the musculoskeletal model, which at the same time is one of the reasons our study was needed. Simulation-based PF translations were estimated using forward dynamics, in which the translations were a function of muscle and ligament forces and cartilage contact. The only marker data used to calculate these forces and contacts, was data describing tibiofemoral flexion. This highlights the value of the method we presented in this study: marker grid-based PF translations (OMC_GRID) of even only one direction could be used as marker input describing the patella. Adding this complementary kinematic data could improve the model accuracy. Future research should evaluate the effect and validity of using marker grid data for existing musculoskeletal simulation models. Ideally, subject-specific cartilage geometries (obtained by one static CT or MRI scan) would be used for these simulations since cartilage geometries largely determine PF kinematics [56].

Next, our grid-based patellar excursions were similar to those seen in literature (**Table 5**). For example, patellar excursions during KA_ENGAGED for our method in the ML, SI and AP directions were 7mm, 17 mm and 7 mm, while those reported by Seisler and Sheehan [57] (measured during a similar knee angle range: 0° - 43°) were 8 mm, 23 mm and 3 mm. Although other studies investigated larger knee angle ranges (up to 108°), we can still see similar patellar excursions.

In addition to that, our method estimated patellar motion in the ML direction which can be described by a C-shaped pattern, first moving medially followed by laterally as the knee moves from extension towards flexion. This C-shaped curve was also found by cadaveric studies [57, 19],

Table 5. Patellar excursions (mm) reported by studies measuring PF translations. Results of our study (OMC_GRID) are given for both knee angle ranges

Study	Methods	Knee angle range	Peak-to-peak patellar displacement (mm)		
			ML	SI	AP
Amis et al. [57]	Electromagnetic tracking	0° - 90°	12	-	-
Seisler and Sheehan [59]	Dynamic MRI	0° - 43°	8	23	3
Shin et al. [60]	MRI	0° - 40°	5	9	4
Gray et al. [35]	Biplanar videoradiography	0° - 70°	5	15	11
Thomeer et al. [61]	Biplanar videoradiography	9° - 108°	4	15	17
MacIntyre et al. [62]	MRI	0° - 60°	6	31	10
Present study	**Marker grid (KA_ALL)**	**0° - 48°**	**12**	**20**	**13**
	" (KA_ENGAGED)	**20° - 48°**	**7**	**17**	**7**

in vivo studies using MRI [31] or biplanar videoradiography [35] and by a systematic review made by Yu et al. [58].

Limitations and future research

Our method did not correctly track the patella during extended knee angles (< 20°), while many daily activities (e.g. gait) require extended knee positioning. In addition to that, patellar malalignment (i.e. irregular motion of the patella within the trochlear groove) causes most problems during knee extension [63]. As mentioned before, most pain resulting from PF pathologies such as PFOA occur during flexed knee positions, but since motion analysis of both extended and flexed knee positions are desired, future research should focus on improving our method for knee angles lower than 20°.

Patellofemoral rotations were also not calculated by the patella identification algorithm. This is not problematic when using our method to obtain complementary marker information to use as input for a musculoskeletal model. Only two or even one translational degrees of freedom (i.e. ML-, SI-, and AP-translation) are sufficient to improve the estimation of the remaining patellofemoral degrees of freedom using inverse kinematics. This is because the shape of the trochlear groove (i.e. the articulating surface of the femur) largely determines the 3D path of the patella [64]. On the other hand, clinical assessment of patellofemoral pathologies can require information of patellofemoral rotations, considering these were found to differ considerably between healthy and symptomatic knees [62, 64]. Therefore, more work is needed to enable measurement of patellofemoral rotations.

Another problem arises if we consider that the eventual aim of this study is to enable researchers and clinicians to measure patellar motion during daily activities such as gait. Marker grid trajectories were found difficult to track during gait trials, which is problematic since we eventually want to measure PF translations during these motions.

Next, the third step of the patella identification algorithm involved creation of 9000 virtual markers that were used to identify the patellar location. We did not select this number based on a clear rational, besides the fact that it was large enough to provide correct results (as shown by CT_BONES and CT_GRID) while an acceptable computation time of less than 15 seconds per trial was achieved. Future research involving larger data sets could focus on finding the optimal balance between accuracy and computation time.

Next, we identified the 2000 markers with the largest Z-value (i.e. with the largest distance to the marker grid reference frame). This number was chosen to match the patellar dimensions we determined previously using 4D-CT data. This method requires manual determination of virtual marker region size selection for each measured participant, considering individuals have different patellar dimensions. Future research should focus on improving this, for example by shape fitting of the patella on the virtual marker grid [65], but this was beyond the scope of this study.

Finally, since 4D-CT data of only one healthy participant was used, we were not able to perform a proper validation but only demonstrated a proof of concept. Future studies should therefore use more participants and include participants with knee pathology.

5. Conclusion

We developed a new, non-invasive method to measure *in vivo* patellofemoral translations using a grid of skin-mounted markers. Comparison of our grid-based results to those obtained using the gold standard, CT-based approach demonstrated a proof of work (showing that our workflow is feasible). Marker grid-based PF translations were measured with an accuracy of 3 mm for knee angles larger than 20°. Larger errors were seen during extended knee angles (< 20°), so more research is needed to use our method for this knee angle range.

References

[1] Murphy, L., Schwartz, T. A., Helmick, C. G., Renner, J. B., Tudor, G., Koch, G., ... & Jordan, J. M. (2008). Lifetime risk of symptomatic knee osteoarthritis. *Arthritis Care & Research: Official Journal of the American College of Rheumatology*, *59*(9), 1207-1213.

[2] Losina, E., Paltiel, A. D., Weinstein, A. M., Yelin, E., Hunter, D. J., Chen, S. P., ... & Katz, J. N. (2015). Lifetime medical costs of knee osteoarthritis management in the United States: impact of extending indications for total knee arthroplasty. *Arthritis care & research*, *67*(2), 203-215.

[3] Arthritis Foundation. Arthritis by the Numbers: Book of Trusted Facts and Figures; 2017. Available from: https://www.arthritis.org/ Documents/Sections/About-Arthritis/arthritis-facts-stats-figures.pdf. Accessed May 24, 2017.

[4] Blagojevic, M., Jinks, C., Jeffery, A., & Jordan, 1. (2010). Risk factors for onset of osteoarthritis of the knee in older adults: a systematic review and meta-analysis. *Osteoarthritis and cartilage*, *18*(1), 24-33.

[5] Chaudhari, A. M., Briant, P. L., Bevill, S. L., Koo, S., & Andriacchi, T. P. (2008). Knee kinematics, cartilage morphology, and osteoarthritis after ACL injury. *Medicine and science in sports and exercise*, *40*(2), 215-222.

[6] Heidari, B. (2011). Knee osteoarthritis prevalence, risk factors, pathogenesis and features: Part I. *Caspian journal of internal medicine*, *2*(2), 205.

[7] Lankhorst, N. E., van Middelkoop, M., Crossley, K. M., Bierma-Zeinstra, S. M. A., Oei, E. H. G., Vicenzino, B., & Collins, N. J. (2016). Factors that predict a poor outcome 5–8 years after the diagnosis of patellofemoral pain: a multicentre observational analysis. *British journal of sports medicine*, *50*(14), 881-886.

[8] Tanamas, S., Hanna, F. S., Cicuttini, F. M., Wluka, A. E., Berry, P., & Urquhart, D. M. (2009). Does knee malalignment increase the risk of development and progression of knee osteoarthritis? A systematic review. *Arthritis Care & Research: Official Journal of the American College of Rheumatology*, *61*(4), 459-467.

[9] Segal, N. A., Anderson, D. D., Iyer, K. S., Baker, J., Torner, J. C., Lynch, J. A., ... & Brown, T. D. (2009). Baseline articular contact stress levels predict incident symptomatic knee osteoarthritis development in the MOST cohort. *Journal of orthopaedic research*, *27*(12), 1562-1568.

[10] Farrokhi, S., Keyak, J. H., & Powers, C. M. (2011). Individuals with patellofemoral pain exhibit greater patellofemoral joint stress: a finite element analysis study. *Osteoarthritis and Cartilage*, *19*(3), 287-294.

[11] Gustafson, J. A., Elias, J. J., Fitzgerald, G. K., Tashman, S., Debski, R. E., & Farrokhi, S. (2021). Combining advanced computational and imaging techniques as a quantitative tool to estimate patellofemoral joint stress during downhill gait: A feasibility study. *Gait & Posture*, *84*, 31-37.

[12] Yamaguchi, G. T., & Zajac, F. E. (1989). A planar model of the knee joint to characterize the knee extensor mechanism. *Journal of biomechanics*, *22*(1), 1-10.

[13] Wheatley, M. G., Thelen, D. G., Deluzio, K. J., & Rainbow, M. J. (2021). Knee extension moment arm variations relate to mechanical function in walking and running. *Journal of the Royal Society Interface*, *18*(181), 20210326.

[14] Shu, L., Yamamoto, K., Yoshizaki, R., Yao, J., Sato, T., & Sugita, N. (2021). Multiscale finite element musculoskeletal model for intact knee dynamics. *Computers in biology and medicine*, 105023.

[15] Lenhart, R. L., Kaiser, J., Smith, C. R., & Thelen, D. G. (2015). Prediction and validation of load-dependent behavior of the tibiofemoral and patellofemoral joints during movement. *Annals of biomedical engineering*, *43*(11), 2675-2685.

[16] Smith, C. R., Brandon, S. C., & Thelen, D. G. (2019). Can altered neuromuscular coordination restore soft tissue loading patterns in anterior cruciate ligament and menisci deficient knees during walking?. *Journal of Biomechanics*, *82*, 124-133.

[17] Wünschel, M., Leichtle, U., Obloh, C., Wülker, N., & Müller, O. (2011). The effect of different quadriceps loading patterns on tibiofemoral joint kinematics and patellofemoral contact pressure during simulated partial weight-bearing knee flexion. *Knee Surgery, Sports Traumatology, Arthroscopy*, *19*(7), 1099-1106.

[18] Kanamori, A., Woo, S. L., Ma, C. B., Zeminski, J., Rudy, T. W., Li, G., & Livesay, G. A. (2000). The forces in the anterior cruciate ligament and knee kinematics during a simulated pivot shift test: a human cadaveric study using robotic technology. *Arthroscopy: The Journal of Arthroscopic & Related Surgery*, *16*(6), 633-639.

[19] Goudakos, I. G., König, C., Schöttle, P. B., Taylor, W. R., Singh, N. B., Roberts, I., ... & Heller, M. O. (2009). Stair climbing results in more challenging patellofemoral contact mechanics and kinematics than walking at early knee flexion under physiological-like quadriceps loading. *Journal of biomechanics*, *42*(15), 2590-2596.

[20] Wurm, S., Kainz, H., Augat, P., & Reng, W. (2013). The influence of patellar resurfacing on patellar kinetics and retropatellar contact characteristics. *Journal of Orthopaedic Science*, *18*(1), 61-69.

[21] Lin, F., Makhsous, M., Chang, A. H., Hendrix, R. W., & Zhang, L. Q. (2003). In vivo and noninvasive six degrees of freedom patellar tracking during voluntary knee movement. *Clinical biomechanics*, *18*(5), 401-409.

[22] Eichelberger, P., Ferraro, M., Minder, U., Denton, T., Blasimann, A., Krause, F., & Baur, H. (2016). Analysis of accuracy in optical motion capture–A protocol for laboratory setup evaluation. *Journal of biomechanics*, *49*(10), 2085-2088.

[23] Kim, H. Y., Kim, K. J., Yang, D. S., Jeung, S. W., Choi, H. G., & Choy, W. S. (2015). Screw-home movement of the tibiofemoral joint during normal gait: three-dimensional analysis. *Clinics in orthopedic surgery*, *7*(3), 303-309.

[24] Akbarshahi, M., Schache, A. G., Fernandez, J. W., Baker, R., Banks, S., & Pandy, M. G. (2010). Non-invasive assessment of soft-tissue artifact and its effect on knee joint kinematics during functional activity. *Journal of biomechanics*, *43*(7), 1292-1301.

[25] Wilson, N. A., Press, J. M., Koh, J. L., Hendrix, R. W., & Zhang, L. Q. (2009). In vivo noninvasive evaluation of abnormal patellar tracking during squatting in patients with patellofemoral pain. *The Journal of Bone and Joint Surgery. American volume.*, *91*(3), 558.

[26] Laprade, J., & Lee, R. (2005). Real-time measurement of patellofemoral kinematics in asymptomatic subjects. *The Knee*, *12*(1), 63-72.

[27] Draper, C. E., Besier, T. F., Santos, J. M., Jennings, F., Fredericson, M., Gold, G. E., ... & Delp, S. L. (2009). Using real-time MRI to quantify altered joint kinematics in subjects with patellofemoral pain and to evaluate the effects of a patellar brace or sleeve on joint motion. *Journal of Orthopaedic Research*, *27*(5), 571-577.

[28] Charbonnier, C., Chague, S., Kolo, F. C., Chow, J. C. K., & Lädermann, A. (2014). A patient-specific measurement technique to model shoulder joint kinematics. *Orthopaedics & Traumatology: Surgery & Research*, *100*(7), 715-719.

[29] Lädermann, A., Athwal, G. S., Bothorel, H., Collin, P., Mazzolari, A., Raiss, P., & Charbonnier, C. (2021). Scapulothoracic Alignment Alterations in Patients with Walch Type B Osteoarthritis: An In Vivo Dynamic Analysis and Prospective Comparative Study. *Journal of Clinical Medicine*, *10*(1), 66.

[30] Muhle, C., Brossmann, J., & Heller, M. (1999). Kinematic CT and MR imaging of the patellofemoral joint. *European Radiology*, *9*(3), 508-518.

[31] Powers, C. M., Ward, S. R., Fredericson, M., Guillet, M., & Shellock, F. G. (2003). Patellofemoral kinematics during weight-bearing and non-weight-bearing knee extension in persons with lateral subluxation of the patella: a preliminary study. *Journal of Orthopaedic & Sports Physical Therapy*, *33*(11), 677-685.

[32] Adachi, T., Kato, Y., Kiyotomo, D., Kawamukai, K., & Machida, Y. (2021). Accuracy Verification of 4D-CT Analysis of Knee Joint Movements: A Pilot Study Using a Knee Joint Model and Motion-capture System.

[33] Lin, C. C., Lu, T. W., Li, J. D., Kuo, M. Y., Kuo, C. C., & Hsu, H. C. (2020). An automated three-dimensional bone pose tracking method using clinical interleaved biplane fluoroscopy systems: application to the knee. *Applied Sciences*, *10*(23), 8426.

[34] Miranda, D. L., Fadale, P. D., Hulstyn, M. J., Shalvoy, R. M., Machan, J. T., & Fleming, B. C. (2013). Knee biomechanics during a jump-cut maneuver: effects of gender & ACL surgery. *Medicine and science in sports and exercise*, *45*(5), 942.

[35] Gray, H. A., Guan, S., Thomeer, L. T., Schache, A. G., de Steiger, R., & Pandy, M. G. (2019). Three-dimensional motion of the knee-joint complex during normal walking revealed by mobile biplane x-ray imaging. *Journal of Orthopaedic Research®*, *37*(3), 615-630.

[36] Ishimaru, M., Shiraishi, Y., Ikebe, S., Higaki, H., Hino, K., Onishi, Y., & Miura, H. (2014). Three-dimensional motion analysis of the patellar component in total knee arthroplasty by the image matching method using image correlations. *Journal of Orthopaedic Research*, *32*(5), 619-626.

[37] Pitcairn, S., Lesniak, B., & Anderst, W. (2018). In vivo validation of patellofemoral kinematics during overground gait and stair ascent. *Gait & posture*, *64*, 191-197.

[38] Besier, T. F., Gold, G. E., Beaupré, G. S., & Delp, S. L. (2005). A modeling framework to estimate patellofemoral joint cartilage stress in vivo. *Medicine and science in sports and exercise*, *37*(11), 1924.

[39] Ali, A. A., Shalhoub, S. S., Cyr, A. J., Fitzpatrick, C. K., Maletsky, L. P., Rullkoetter, P. J., & Shelburne, K. B. (2016). Validation of predicted patellofemoral mechanics in a finite element model of the healthy and cruciate-deficient knee. *Journal of biomechanics*, *49*(2), 302-309.

[40] Cohen, Z. A., Mow, V. C., Henry, J. H., Levine, W. N., & Ateshian, G. A. (2003). Templates of the cartilage layers of the patellofemoral joint and their use in the assessment of osteoarthritic cartilage damage. *Osteoarthritis and Cartilage*, *11*(8), 569-579.

[41] Delp, S. L., Anderson, F. C., Arnold, A. S., Loan, P., Habib, A., John, C. T., ... & Thelen, D. G. (2007). OpenSim: open-source software to create and analyze dynamic simulations of movement. *IEEE transactions on biomedical engineering*, *54*(11), 1940-1950.

[42] Xu, H., Bloswick, D., & Merryweather, A. (2015). An improved OpenSim gait model with multiple degrees of freedom knee joint and knee ligaments. *Computer methods in biomechanics and biomedical engineering*, *18*(11), 1217-1224.

[43] Schmitz, A., & Piovesan, D. (2016). Development of an open-source, discrete element knee model. *IEEE Transactions on Biomedical Engineering*, *63*(10), 2056-2067.

[44] Marieswaran, M., Sikidar, A., Goel, A., Joshi, D., & Kalyanasundaram, D. (2018). An extended OpenSim knee model for analysis of strains of connective tissues. *Biomedical engineering online*, *17*(1), 1-13.

[45] Killen, B. A., da Luz, S. B., Lloyd, D. G., Carleton, A. D., Zhang, J., Besier, T. F., & Saxby, D. J. (2021). Automated creation and tuning of personalised muscle paths for OpenSim musculoskeletal models of the knee joint. *Biomechanics and Modeling in Mechanobiology*, *20*(2), 521-533.

[46] Grood, E. S., & Suntay, W. J. (1983). A joint coordinate system for the clinical description of three-dimensional motions: application to the knee. *Journal of biomechanical engineering*, *105*(2), 136-144.

[47] Fedorov A., Beichel R., Kalpathy-Cramer J., Finet J., Fillion-Robin J-C., Pujol S., Bauer C., Jennings D., Fennessy F., Sonka M., Buatti J., Aylward S.R., Miller J.V., Pieper S., Kikinis R. 3D Slicer as an Image Computing Platform for the Quantitative Imaging Network. Magnetic Resonance Imaging. 2012 Nov;30(9):1323-41. PMID: 22770690.

[48] Chen, H., Kluijtmans, L., Bakker, M., Dunning, H., Kang, Y., Van De Groes, S., ... & Verdonschot, N. (2020). A robust and semi-automatic quantitative measurement of patellofemoral instability based on four dimensional computed tomography. *Medical engineering & physics*, *78*, 29-38.

[49] Miranda, D. L., Rainbow, M. J., Leventhal, E. L., Crisco, J. J., & Fleming, B. C. (2010). Automatic determination of anatomical coordinate systems for three-dimensional bone models of the isolated human knee. *Journal of biomechanics*, *43*(8), 1623-1626.

[50] Rainbow, M. J., Miranda, D. L., Cheung, R. T., Schwartz, J. B., Crisco, J. J., Davis, I. S., & Fleming, B. C. (2013). Automatic determination of an anatomical coordinate system for a three-dimensional model of the human patella. *Journal of biomechanics*, *46*(12), 2093-2096.

[51] https://simtk.org/projects/opensim-jam

[52] Smith, C. R., Won Choi, K., Negrut, D., & Thelen, D. G. (2018). Efficient computation of cartilage contact pressures within dynamic simulations of movement. *Computer Methods in Biomechanics and Biomedical Engineering: Imaging & Visualization*, *6*(5), 491-498.

[53] Thelen, D. G., Won Choi, K., & Schmitz, A. M. (2014). Co-simulation of neuromuscular dynamics and knee mechanics during human walking. *Journal of biomechanical engineering*, *136*(2), 021033.

[54] Colvin, A. C., & West, R. V. (2008). Patellar instability. *Jbjs*, *90*(12), 2751-2762.

[55] Akoglu, H. (2018). User's guide to correlation coefficients. *Turkish journal of emergency medicine*, *18*(3), 91-93.

[56] Macri, E. M., Stefanik, J. J., Khan, K. K., & Crossley, K. M. (2016). Is tibiofemoral or patellofemoral alignment or trochlear morphology associated with patellofemoral osteoarthritis? A systematic review. *Arthritis care & research*, *68*(10), 1453-1470.

[57] Amis, A. A., Senavongse, W., & Bull, A. M. (2006). Patellofemoral kinematics during knee flexion-extension: An in vitro study. *Journal of orthopaedic research*, *24*(12), 2201-2211.

[58] Yu, Z., Yao, J., Wang, X., Xin, X., Zhang, K., Cai, H., ... & Yang, B. (2019). Research methods and progress of patellofemoral joint kinematics: a review. *Journal of healthcare engineering*, *2019*.

[59] Seisler, A. R., & Sheehan, F. T. (2007). Normative three-dimensional patellofemoral and tibiofemoral kinematics: a dynamic, in vivo study. *IEEE Transactions on biomedical engineering*, *54*(7), 1333-1341.

[60] Shin, C. S., Carpenter, R. D., Majumdar, S., & Ma, C. B. (2009). Three-dimensional in vivo patellofemoral kinematics and contact area of anterior cruciate ligament–deficient and–reconstructed subjects using magnetic resonance imaging. *Arthroscopy: The Journal of Arthroscopic & Related Surgery*, *25*(11), 1214-1223.

[61] Thomeer, L., Guan, S., Gray, H., Schache, A., de Steiger, R., & Pandy, M. (2021). Six-degree-of-freedom tibiofemoral and patellofemoral joint motion during activities of daily living. *Annals of Biomedical Engineering*, *49*(4), 1183-1198.

[62] MacIntyre, N. J., Hill, N. A., Fellows, R. A., Ellis, R. E., & Wilson, D. R. (2006). Patellofemoral joint kinematics in individuals with and without patellofemoral pain syndrome. *JBJS*, *88*(12), 2596-2605.

[63] McNally, E. G., Ostlere, S. J., Pal, C., Phillips, A., Reid, H., & Dodd, C. (2000). Assessment of patellar maltracking using combined static and dynamic MRI. *European radiology*, *10*(7), 1051-1055.

[64] Katchburian, M. V., Bull, A. M., Shih, Y. F., Heatley, F. W., & Amis, A. A. (2003). Measurement of patellar tracking: assessment and analysis of the literature. *Clinical Orthopaedics and Related Research (1976-2007)*, *412*, 241-259.

[65] Lempitsky, V., & Boykov, Y. (2007, June). Global optimization for shape fitting. In *2007 IEEE Conference on Computer Vision and Pattern Recognition* (pp. 1-8). IEEE.

[66] Fregly, B. J., Bei, Y., & Sylvester, M. E. (2003). Experimental evaluation of an elastic foundation model to predict contact pressures in knee replacements. *Journal of biomechanics*, *36*(11), 1659-1668.

[67] Bland, J. M., & Altman, D. (1986). Statistical methods for assessing agreement between two methods of clinical measurement. *The lancet*, *327*(8476), 307-310.

[68] Patel, V. V., Hall, K., Ries, M., Lindsey, C., Ozhinsky, E., Lu, Y., & Majumdar, S. (2003). Magnetic resonance imaging of patellofemoral kinematics with weight-bearing. *JBJS*, *85*(12), 2419-2424.

[69] Loudon, J. K. (2016). Biomechanics and pathomechanics of the patellofemoral joint. *International journal of sports physical therapy*, *11*(6), 820.